Chinese Chemical Letters 37 (2026) 111865

Contents lists available at ScienceDirect

Chinese Chemical Letters

journal homepage: www.elsevier.com/locate/cclet

Recent progress on the (photo)electrocatalytic molecular oxygen activation in reactive oxygen species generation for environmental remediation

Limin Jin[a], Jie Xu[c], Huayue Zhu[b], Chunjuan Li[a,*], Zhengfeng Hu[d,*], Qi Wang[a,*]

[a] Zhejiang Key Laboratory of Solid Waste Pollution Control and Resource Utilization, School of Environmental Science and Engineering, Zhejiang Gongshang University, Hangzhou 310012, China
[b] Institute of Environmental Engineering Technology, Taizhou University, Taizhou 318000, China
[c] Hangzhou Iron&Steel Group Co., LTD, Hangzhou 310022, China
[d] Ecological and Environmental Science and Research Institute of Zhejiang Province, Hangzhou 310007, China

ARTICLE INFO

Article history:
Received 29 April 2025
Revised 7 August 2025
Accepted 20 September 2025
Available online 21 September 2025

Keywords:
Molecular oxygen
Reactive oxygen species
(Photo)electrocatalyst
(Photo)electrocatalytic reactor
Environmental remediation

ABSTRACT

Molecular oxygen (O_2) activation offers a sustainable pathway for environmental remediation by generating reactive oxygen species (ROS), yet challenges in efficiency, stability, and scalability hinder its practical application. This review systematically explores recent advances in integrated (photo)electrocatalytic systems, where synergistic coupling of photonic and electrical energy inputs overcomes spin-forbidden barriers in molecular O_2 activation. Emphasis is placed on nanoscale catalyst engineering, including alloy, carbon-based materials, and single-atom catalysts, to precisely regulate ROS generation *via* electronic structure design and targeted electron transfer. Parallel innovations in reactor design, such as flow-by and flow-through (photo)electrodes, are analyzed for their role in enhancing mass transport, increasing ROS yields, and ensuring operational durability. Integrating fundamental insights with system engineering, the review provides a roadmap for advancing energy-efficient (photo)electrocatalytic platforms, highlighting their transformative potential in ROS-mediated environmental technologies.

© 2026 Published by Elsevier B.V. on behalf of Chinese Chemical Society and Institute of Materia Medica, Chinese Academy of Medical Sciences.

1. Introduction

Advanced oxidation processes (AOPs) have become indispensable in environmental remediation, achieving pollutant removal through the generation of highly reactive oxygen species (ROS) [1,2]. These ROS, including superoxide ($O_2^{\bullet-}$), hydroxyl radicals ($^{\bullet}OH$), and singlet oxygen ($^1O_2$), are typically derived from chemical precursors like hydrogen peroxide (H_2O_2), ozone (O_3), or peroxymonosulfate (PMS) [3,4]. While effective, the reliance on these precursors poses challenges due to their costly synthesis, unstable storage, and energy-intensive transport. In contrast, molecular oxygen (O_2), a naturally abundant and eco-friendly oxidant constituting 21 % of the air by volume, holds immense potential for sustainable environmental applications [5]. However, its practical utilization in AOPs remains constrained by inherent stability, where its triplet ground state and high-energy molecular orbitals prevent direct interaction with most organic pollutants [6]. Consequently, only a small fraction (<5 %) of molecular O_2 in reaction systems is catalytically converted into ROS, starkly contrasting with the high efficiency achieved by synthetic precursors like H_2O_2 or O_3 [7,8]. Consequently, overcoming these limitations requires innovative strategies to activate molecular O_2 under ambient conditions, thereby unlocking its full potential as a sustainable ROS source.

Conventional methods for molecular O_2 activation, including physical, chemical, and biological approaches, have been widely used to generate ROS for environmental remediation [9,10]. Despite their utility, these approaches often suffer from critical limitations, such as energy-intensive operations, secondary pollutant formation, and unsatisfactory activation efficiency, which hinder their practical application [11,12]. In response, (photo)electrocatalytic activation of molecular O_2 have emerged as a breakthrough strategy [13,14]. By synergistically integrating photonic and electrical energy, this approach breakthrough the inherent spin limitations of triplet-state molecular O_2, enabling efficient ROS generation under mild conditions [15]. A key advantage of (photo)electrocatalytic systems is their compatibility with renewable energy inputs, such as solar or wind power, which ensures cost-effective scalability for large-scale environmental remediation [16,17]. Therefore, the main

* Corresponding authors.
E-mail addresses: lichunjuan@zjgsu.edu.cn (C. Li), huzhengfeng2003@163.com (Z. Hu), wangqi8327@zjgsu.edu.cn (Q. Wang).

https://doi.org/10.1016/j.cclet.2025.111865
1001-8417/© 2026 Published by Elsevier B.V. on behalf of Chinese Chemical Society and Institute of Materia Medica, Chinese Academy of Medical Sciences.

orientation of this paper is the analysis of molecular O_2 activation *via* (photo)electrocatalytic system, offering a sustainable pathway to mitigate pollution.

Recent reviews for molecular O_2 activation have predominantly concentrated on catalyst design, with particular emphasis on optimizing electronic properties and electron transfer through advanced strategies, including defect engineering, heterojunction construction, and nanoconfinement [18,19]. For instance, N-doped carbon electrodes derived from N-rich chitosan demonstrated enhanced molecular O_2 activation, where pyridinic and graphitic N sites doubled $^{\bullet}OH$ and $O_2^{\bullet-}$ concentrations, enabling efficient degradation of persistent pollutants like perfluorooctanoic acid in complex aqueous environments [20]. Similarly, MIL-101(Fe)-based Z-scheme heterojunctions exhibited robust photocatalytic activity, generating $O_2^{\bullet-}$, $^{\bullet}OH$, and $^1O_2$ to drive pollutant degradation [21]. While, seldom of the reviews have targeted at the state-of-the-art (photo)electrocatalysts together with the (photo)electrochemical device designs for molecular O_2 activation. By addressing these limitations, this review bridges the disconnect between material-centric studies and device engineering, offering a holistic perspective on (photo)electrocatalytic molecular O_2 activation.

Herein, we provide a thorough summary and in-depth analysis of current research on molecular O_2 activation utilizing (photo)electrocatalysts and (photo)electrochemical devices, with an emphasis on enhancing mass and electron transfer for the on-site production of ROS. Specifically, the reaction mechanisms, advantages, and disadvantages of (photo)electrochemical device designs, particularly those incorporating catalyst engineering, are analyzed in detail. By connecting fundamental science with practical engineering considerations, this work aims to inspire the development of robust, scalable technologies for ROS generation toward environmental remediation.

2. Analysis of the molecular O_2 activation pathway

ROS are broadly classified into two types: radicals (*e.g.*, $O_2^{\bullet-}$ and $^{\bullet}OH$) and nonradicals (*e.g.*, H_2O_2 and $^1O_2$). The ground-state molecular O_2 ($^3\Sigma_g^-$) exists in its lowest energy configuration, characterized by two unpaired electrons in antibonding orbitals with parallel spins (Figs. 1A and B) [22,23]. Contrast, excited-state oxygen species, such as O_2 ($^1\Delta_g$) and O_2 ($^1\Sigma_g^+$), possess distinct electronic configurations. In the O_2 ($^1\Delta_g$) state, electrons pair within the same orbital, whereas in the higher-energy O_2 ($^1\Sigma_g^+$) state, occupy separate orbitals with opposite spins. The O_2 ($^1\Sigma_g^+$) state is highly unstable and short-lived, rapidly decaying to the lower-energy O_2 ($^1\Delta_g$) state, which corresponds to the widely studied $^1O_2$ [23,24]. Additionally, $O_2^{\bullet-}$ and $^{\bullet}OH$ are often less stable than nonradicals because they contain a single unpaired electron.

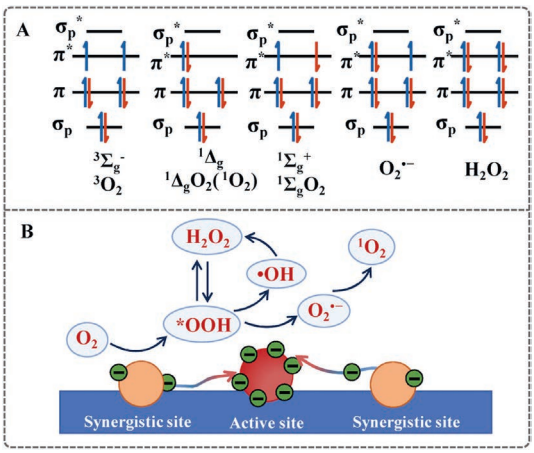


Fig. 1. (A) Molecular orbital diagrams for a ground-state triplet O_2 molecule, two types of $^1O_2$, $O_2^{\bullet-}$ and H_2O_2. Copied with permission [23]. Copyright 2013, Wiley. (B) Possibly the relationship or differences in generating different ROS.

2.1. Superoxide radical anion ($O_2^{\bullet-}$)

$O_2^{\bullet-}$ is a highly reactive intermediate formed when molecular O_2 undergoes single-electron reduction. Structurally, the O–O bond in $O_2^{\bullet-}$ (1.28–1.33 Å) is slightly elongated than that of ground-state O_2 (1.21 Å) due to the addition of an electron [25]. This structural enhances its instability and reactivity, enabling $O_2^{\bullet-}$ act as both an oxidant and a reductant across a broad redox potential range (−0.35 V to +0.94 V) in photo(electro)catalytic systems. As shown in Fig. 2A, a notable example involves Fe atoms coordinated within N-rich carbon frameworks (Fe–N_4), which can stabilize molecular O_2 adsorption and facilitate electron transfer from the Fe sites to O_2, yielding $O_2^{\bullet-}$ for ethylbenzene oxidation [26]. Although single-electron oxygen reduction dominates its formation, $O_2^{\bullet-}$ also serves as a precursor to other ROS, including H_2O_2 and $^1O_2$, through further reduction or coupling steps. By optimizing electron transfer mechanisms and stabilizing reactive intermediates, catalytic systems can be engineered to enhance $O_2^{\bullet-}$ generation and environmental remediation processes.

2.2. Singlet oxygen ($^1O_2$)

$^1O_2$ is an energized form of the molecular O_2, which was produced by elevating ground-state oxygen ($^3\Sigma_g^-$) to higher-energy configurations [27]. Two distinct excited states are possible: the lower-energy $^1\Delta$g state (95 kJ/mol) and the higher-energy $^1\Sigma_g^+$ state (158 kJ/mol). The $^1\Delta_g$ state forms when two electrons with opposing spins occupy the same π orbital, whereas the $^1\Sigma_g^+$ state arises when these electrons occupy separate orbitals [28]. Due to spin conservation constraints, transitions from the $^1\Delta_g$ to the $^1\Sigma_g^+$ state are prohibited. In contrast, the $^1\Sigma_g^+$ state can revert to the ground state through a permitted transition, leaving the $^1\Delta$g state relatively stable as "$^1O_2$" [29]. For instance, Jiang *et al.* demonstrated that alloying Co with Fe promotes electron transfer from Co to Fe, creating electron-deficient Co sites that efficiently catalyze O_2-to-$^1O_2$ conversion in flow-through systems Fig. 2B) [30]. However, the efficiency of $^1O_2$ production is constrained by the fleeting lifespan of excited-state species, which limits their ability to drive molecular O_2 activation. Addressing this challenge requires strategies to stabilize these transient states, thereby improving the overall yield and utility of $^1O_2$ in environmental remediations.

2.3. Hydroxyl radical ($^{\bullet}OH$)

$^{\bullet}OH$ consist of a H atom bonded to an O atom, enabling them to extract H atoms from surrounding molecules to form water, thereby destabilizing contaminants [31]. The activation of molecular O_2 to generate $^{\bullet}OH$ typically begins with a one-electron reduction step, producing $O_2^{\bullet-}$. These intermediates can follow two primary pathways: direct dissociation and hydrogenation to form $^{\bullet}OH$, or further reduction and hydrogenation to yield H_2O_2. The latter route is often kinetically favorable, as it avoids the energy-intensive cleavage of the O–O bond, with H_2O_2 subsequently reacting with Fe^{2+} or other transition metal ions in a Fenton-like process to produce $^{\bullet}OH$. Recent advances highlight that coupling transition metals (*e.g.*, Fe, Co, Ni, Cu) with carbon-based materials can precisely tune the selectivity of $^{\bullet}OH$ generation *via* 3e$^-$ oxygen reduction reaction (ORR) [5]. For example, Xiao *et al.* developed a carbon aerogel embedded with a core-shell FeCo alloy, where carboxyl groups on the carbon surface promoted H_2O_2 production *via*

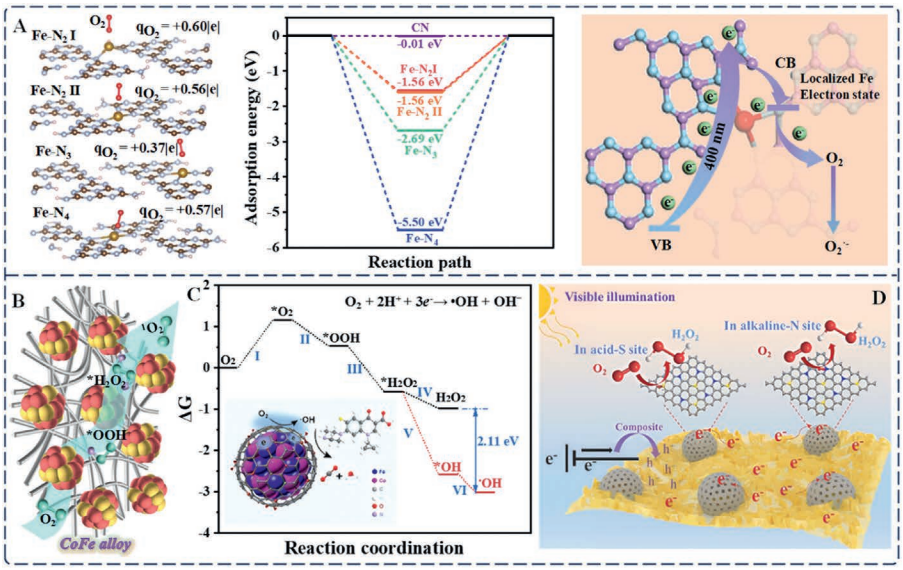


Fig. 2. (A) Calculated charge difference surfaces of the Fe–N_x coordination systems, calculated energy of molecular O_2 adsorption on different sites, and schematic illustration of O_2 to $O_2^{\bullet-}$. Copied with permission [26]. Copyright 2013, Wiley. (B) Proposed electrocatalytic activation mechanism of molecular O_2 to $^1O_2$ over the CoFeCNT filter. Copied with permission [30]. Copyright 2025, Elsevier. (C) Selective electrocatalytic reduction of O_2 to $^{\bullet}OH$ *via* 3e$^-$ pathway with FeCo alloy encapsulated carbon aerogel. Copied with permission [32]. Copyright 2021, Wiley. (D) Binary heteroatom dopants enable carbon-based heterostructures for efficient (photo)electrocatalytic O_2 to H_2O_2 synthesis. Copied with permission [36]. Copyright 2024, Elsevier.

the 2e$^-$ ORR pathway, while electrons from the FeCo alloy facilitated the reduction of H_2O_2 to $^{\bullet}OH$ through a 1e$^-$ process by altering the local electronic environment of the carbon shell (Fig. 2C) [32]. This cascade mechanism, converting O_2 to $^{\bullet}OH$ through 3e$^-$ ORR process, overcomes the slow electron transfer bottleneck in traditional Fenton redox cycles, significantly improving efficiency.

2.4. Hydrogen peroxide (H_2O_2)

H_2O_2, in which the two O atoms are bonded *via* a shared electron pair, forms an inherently unstable and transient –O–O– structural unit, serving as both oxidizing and reducing agents [33]. Utilizing solar energy and O_2 as feedstocks, photo(electro)catalytic H_2O_2 generation surpasses traditional photocatalysis in solar energy conversion efficiency and requires less electrical input than standalone electrocatalysis [34]. Photocathodes absorb light and produce carriers (e$^-$ and h$^+$), which are transferred to the catalyst surface. Molecular O_2 initially combines with 1e$^-$ to form $O_2^{\bullet-}$, which subsequently react with 2H$^+$ and another 1e$^-$ to produce H_2O_2 *via* a two-step 1e$^-$ transfer pathway [35]. Alternatively, O_2 directly interacts with 2e$^-$ and 2H$^+$ to generate H_2O_2 through 2e$^-$ transfer mechanism. Recent work by Zhu *et al.* demonstrated a metal-free carbon-based heterostructure material with N, S co-doping, in which binary heteroatom-doped carbon spheres are loaded onto carbon nitride polymer (Fig. 2D) [36]. Theoretical calculations and experimental results reveal that S- and N-sites suppress O–O cleavage and facilitate *OOH formation through their respective subtle microenvironments, mediating superior 2e$^-$ ORR selectivity for H_2O_2 production in acidic and alkaline conditions. A critical challenge in H_2O_2 (photo)electrosynthesis lies in suppressing H_2O_2 self-decomposition. Mitigation strategies include physically isolating H_2O_2 from the counter electrode to minimize unwanted reactions or converting H_2O_2 into stable peroxide salts to reduce decomposition while enabling controlled release, storage, and transport.

3. The (photo)electrocatalysts for molecular O_2 activation

Advances in synthesis techniques and computational modeling have enabled the development of diverse (photo)electrocatalysts, including metal alloys, single-atom materials, and carbon-based systems, to drive the activation of molecular O_2 for ROS generation.

3.1. Metal and alloy catalysts

Noble metals, such as Au, Ag, Pd, and Pt, are widely studied in molecular O_2 activation within (photo)electrocatalytic systems [37]. However, their high binding affinity to molecular O_2 often demands significant energy input, creating a trade-off between catalytic activity and selectivity. To address this, researchers have engineered noble metal alloys, which adjust the O-binding properties to enhance catalytic performance by incorporating secondary metals. For example, Pd-Ag, Pd-Cu, Pt-Mn, and Au-Pd/ZnO hybrid systems exhibit superior molecular O_2 activation compared to single-metal catalysts, as demonstrated by experimental and theoretical studies [38,39]. As illustrated in Fig. 3A, analyses of the stable O_2 adsorption configurations and dissociation pathways on PdCu alloy surfaces reveal a composition-dependent trend: O_2 adsorption strength increases with higher Cu content but weakens when Cu exceeds Pd stoichiometry [39]. This behavior arises from the higher O_2 adsorption energy of Pd sites relative to Cu, confirming Pd as the preferential adsorption center in the alloy. Further innovation involves tailoring redox-active interfaces. Yang *et al.* designed a $CuBi_2O_4$ photocathode that exploits alternating Cu^+/Cu^{2+} states to drive sequential molecular O_2 activation: Photogenerated electrons reduce O_2 at Cu^{2+} sites to form $O_2^{\bullet-}$, which then react with protons and electrons to produce H_2O_2, an intermediate that subsequently interacts with Cu^+ to yield $^{\bullet}OH$ [40]. Another promising strategy involves nanoscale engineering of catalysts. Reducing metal nanoparticles to ultrasmall sizes, such as Pt clusters anchored on porous supports, significantly increases surface area, and improves selectivity, thereby enhancing the activation efficiency of molecular O_2 [41,42]. However, subsequent research should focus on the challenges of precious metal scarcity/cost, susceptibility to surface poisoning by intermediates (*e.g.*, *OH, OOH), and controlling alloy homogeneity. Collectively, advancements in alloy design, nanostructure, and redox mediation highlight a multifaceted pathway toward developing scalable, energy-efficient systems for optimized molecular O_2 activation.

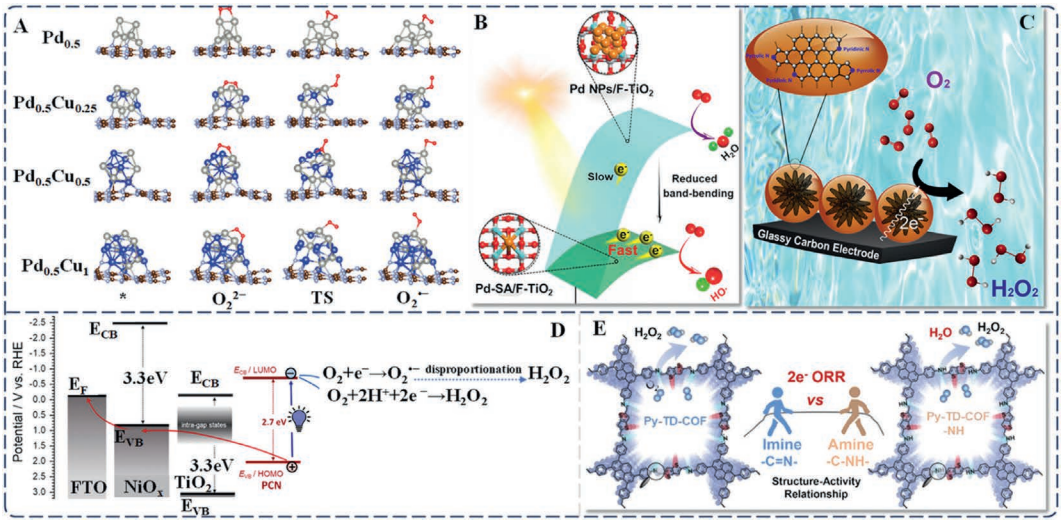


Fig. 3. (A) Transition states in the O_2 dissociation on four PdCu alloy surfaces. Copied with permission [39]. Copyright 2024, ACS. (B) Mechanism for (photo)electrocatalytic O_2 to •OH over Pd-SA/F-TiO_2 and Pd NPs/F-TiO_2. Copied with permission [49]. Copyright 2024, ACS. (C) N-doped graphitized carbon nanohorns in highly selective O_2 to H_2O_2. Copied with permission [54]. Copyright 2018, Elsevier. (D) The scheme for O_2 to H_2O_2 at NiO_x-TiO_2-PCN photocathode. Copied with permission [56]. Copyright 2023, Elsevier. (E) The mechanism of O_2 to H_2O_2 on Py-TD-COF and Py-TD-COF-NH. Copied with permission [59]. Copyright 2024, Elsevier.

3.2. Single atoms catalysts (SACs)

SACs, characterized by near-complete metal atom utilization, have emerged as a promising platform for efficient molecular O_2 activation [43,44]. Their exceptional catalytic performance stems from the ability to precisely control electronic properties by tailoring interactions between isolated metal atoms and their support materials, which enhances the adsorption and activation of molecular O_2 and regulates its dissociation pathway to selectively form ROS [45,46]. Until now, various SACs based on different metals, including Fe, Co, Mn, Pt, and Pd, has been investigated for activation of molecular O_2 toward ROS generation [47]. Furthermore, modifying the coordination environment of SACs with heteroatom (*e.g.*, N, O, S) optimizes electron density at active sites, further improving molecular O_2 activation efficiency [48]. For instance, Zhang *et al.* developed a F-modified TiO_2 catalyst with single Pd atoms bonded to F and O atoms [49]. This configuration promoted the $2e^-$ ORR to H_2O_2 generation with up to 99 % selectivity, while the additional channel bond HO−O···Pd−F−TiO_2 facilitates the photogenerated electron transfer from the conduction band to Pd sites, reducing Pd···O−OH to •OH (Fig. 3B). Similarly, Qin *et al.* designed carbon-supported Ni SACs (Ni SA@C) featuring dual catalytic sites, where the Ni–N_4 (−2.70 eV) sites exhibited stronger adsorption energy for molecular O_2 than that of Ni–N_2O_2 sites (−1.59 eV), suggesting superior molecular O_2 activation at Ni–N_4 sites [50]. This was complemented by planar-averaged charge density difference analyses along the Z-direction, revealing facilitated directional electron transfer from Ni–N_4 sites to O_2 for ROS generation. Subsequent studies should focus on the limitations of SACs, such as stability issues (metal leaching/aggregation) and sensitivity to the coordination environment, where suboptimal ligand bonding can affect performance. These examples underscore how strategic engineering of SACs at the atomic scale can optimize interfacial adsorption and charge transfer dynamics, significantly advancing (photo)electrochemical systems for molecular O_2 activation.

3.3. Carbon-based catalysts

The high cost and limited durability of noble metal-based catalysts under harsh operational conditions remain significant barriers to their widespread adoption [51,52]. In response, carbon-based materials have gained prominence as cost-effective alternatives for molecular O_2 activation, offering robust stability and competitive catalytic performance for ROS generation [53]. For instance, defect-engineered polymeric carbon nitrides, where structural vacancies serve as active sites, efficiently adsorbs and directly converts molecular O_2 into H_2O_2 (Fig. 3C) [54]. Chemical doping of carbon materials further enhances their electronic properties, with catalytic activity dependent on the type and concentration of dopants. Chen *et al.* showed that carbonyl group-functionalized carbon nanotubes lower the energy barrier for molecular O_2 activation, thereby enhancing the production of $^1O_2$, $O_2^{\bullet-}$, and •OH, with $^1O_2$ generation remaining stable across a broad pH range (7–11) [55]. Similarly, Braun *et al.* achieved unprecedented H_2O_2 yields using thermally treated carbon catalysts derived from polydopamine, attributing this success to optimized microporous structures and balanced $N_{pyridinic}/N_{pyrrolic}$ ratios during synthesis (Fig. 3D) [56]. Besides N doping, incorporating heteroatoms like B, F, and S, have also been incorporated to improve the efficiency and selectivity of molecular O_2 activation.

Among them, covalent organic frameworks (COFs), a class of porous carbon polymers with high surface areas and tunable pore structures, exhibit exceptional thermal and structural stability during molecular O_2 activation [57,58]. For instance, imine-linked COFs, which feature electron donor-acceptor characteristics, demonstrated 80 %–92 % selectivity for H_2O_2 production at low operating voltages (0.2–0.7 V *vs.* RHE) (Fig. 3E) [59]. Experimental and computational studies revealed that amine linkages in these frameworks promote H-bonding, elongating, and weakening O–O bonds to facilitate hydrogenation and enhance H_2O_2 selectivity in (photo)electrocatalytic systems. Current optimization strategies focus on tailoring functional groups, incorporating heteroatoms, and engineering linkage chemistry, all of which directly modulate catalytic pathways. Nevertheless, scalability remains constrained by complex synthetic requirements and limited electrical conductivity.

3.4. (In)organic semiconductor photocathodes

Organic variants, such as H-bonded frameworks and polyterthiophene polymers, contrast with inorganic counterparts like such as $CuBi_2O_4$, Cu_3BiS_3, and CuS/MnS. For example, Feng *et al.* designed a Cu-coordinated carbon-nitride (CuCN) photocathode, where Cu-N_2-C active sites reduced the energy barrier for critical reaction intermediates, significantly enhancing molecular O_2

Table 1
Summary of ROS yields and their detection by photocatalysts applying different detection method.

Catalyst	Main ROS	Activity (mA/cm^2)	Durability	Ref.
$B_{0.05}$-C_3N_4	$O_2^{\bullet-}$, $^1O_2$	/	3 h	[62]
GBN	$^1O_2$	3 V *vs.* RHE	2 h	[63]
MoS_2/GDY-3	H_2O_2	/	4 h	[64]
Co_3O_4-TiO_2	H_2O_2	1.23 V *vs.* RHE	4 h	[65]
Cu_xO@C	$O_2^{\bullet-}$, $^{\bullet}OH$	−0.1 V *vs.* RHE	3 h	[66]
Cu/TiO_2	$O_2^{\bullet-}$	−0.1 V *vs.* RHE	14 h	[67]
Gd-doped $BiVO_4$	H_2O_2	3.0 V *vs.* RHE	3 h	[68]
Ni$(OH)_2$/Ni foam	$^{\bullet}OH$	1.60 V *vs.* RHE	40 h	[69]
Cu_2O/CuO	$^{\bullet}OH$	2.2 V *vs.* RHE	8 h	[70]

activation for the generation of $^{\bullet}OH$ and $^1O_2$ *via* Cu-N_2-C active sites [60]. This approach improved efficiency by balancing charge transfer and catalytic activity. Sun *et al.* demonstrated this by integrating a $NaCo_2O_4$ layer beneath $CuBi_2O_4$, synergizing photothermal and photoelectric effects [61]. Under light exposure, this configuration created an internal electric field that boosted charge separation, achieving a notable H_2O_2 yield of 1192.9 μmol/L within 50 min. Such designs underscore the potential of hybrid systems to overcome limitations in charge-carrier dynamics. Beyond these strategies, Schottky junctions have emerged as promising candidates due to their ability to enhance charge separation [11]. These junctions form when semiconductors with differing work functions interact, driving electron transfer until equilibrium, which minimizes electron recombination, enhances charge separation, and further improves molecular O_2 activation. In addition to these approaches, researchers have explored oxides, chalcogenides, anthraquinone-based compounds, and molecular catalysts (Table 1) [62–70], all demonstrating strong molecular O_2 activation capabilities. These materials leverage diverse mechanisms, from bandgap engineering to surface modification, offering versatile pathways to improve molecular O_2 activation.

4. Strategies to improve the stability of (photo)electrocatalysts

The stability of (photo)electrocatalysts is influenced by three primary factors: Catalyst composition, reaction conditions, and reactor design. Optimizing the catalyst itself presents a cost-effective pathway to enhance operational longevity without requiring costly infrastructure upgrades.

4.1. Coating on oxide supports

A promising strategy involves coating catalytic sites onto supports, such as TiO_2, ZnO, or SiO_2. These supports offer high surface area and structural stability, which help to anchor active sites and prevent leakage. While non-oxide supports (*e.g.*, carbon nanotubes) may offer higher conductivity, their vulnerability to corrosion often results in activity loss in acidic O_2-rich environments. Thus, oxides remain preferred for long-term molecular O_2 activation. For example, Lyu *et al.* demonstrated that a carbon-coated TiO_{2-x} support stabilized interfacial oxygen vacancies, enabling activate molecular O_2 into $^1O_2$ or $O_2^{\bullet-}$ during a 12 h of light exposure (Fig. 4A) [71]. Similarly, Zhang *et al.* addressed the challenge of Au nanoparticle sintering by applying a thin SiO_2 layer to Au/TiO_2 [72]. This modification not only prevented agglomeration but also enhanced molecular O_2 activation efficiency under prolonged operation. Protective oxide coatings mitigate structural hydrolysis, collapse, and metal leaching, thereby preserving catalytic activity. However, the coating method must be carefully tailored to ensure compatibility between the active sites, support material, and operational environment. For example, excessive coating thickness or improper thermal treatment during synthesis can block active sites or induce stress fractures. Thereby balancing material compatibility with functional design, these strategies pave the way for durable, high-performance (photo)electrocatalysts in molecular O_2-driven systems.

4.2. Strengthening metal-substrate interaction

The prolonged catalytic performance of materials used in molecular O_2 activation can be substantially enhanced by optimizing the interaction between catalytic sites and their supporting substrates. Key approaches, such as heteroatom doping, oxygen vacancy engineering, and interfacial modifications, which mitigate structural collapse including metal leaching or agglomeration.

Heteroatoms doping: Incorporating heteroatoms such as N, B, and S into catalyst frameworks has proven effective in stabilizing catalytic sites. For instance, N-doped Cu-carbon aerogel electrodes create a N_4-Cu-OOH interface that selectively generates $^1O_2$ at concentrations up to 2583 μmol/L during molecular O_2 activation, while maintaining 98 % efficiency over 50 operational cycles (Fig. 4B) [73]. Additionally, doping can also introduce redox-active metal pairs, such as Fe^{3+}/Fe^{2+} and Mo^{4+}/Mo^{6+}, which directly participate in molecular O_2 activation. The Fe^{3+}/Fe^{2+} pair facilitates the one-electron reduction of O_2 to $O_2^{\bullet-}$, while Mo^{4+}/Mo^{6+} further converts $O_2^{\bullet-}$ to $^1O_2$ (Fig. 4C) [74]. Research should focus how to precisely control the dopant species at the molecular level during the preparation process and adjust the distribution of different species according to the specific requirement and goals.

Oxygen vacancies (OVs): OVs, defects created by missing O atoms in metal oxide lattices, enhance molecular O_2 activation by altering surface electronic states and improving charge transfer for surface reactivity [75]. For example, Mao *et al.* reported that C-doped BiO_{2-x}, engineered with abundant surface OVs and bulk oxygen substitutions, synergistically strengthened molecular O_2 adsorption and charge carrier separation for boosting photocatalytic $O_2^{\bullet-}$ generation (Fig. 4D) [76]. In another study, Yang *et al.* synthesized SnO_2 catalysts with abundant OVs, which demonstrated higher oxygen evolution potentials and faster electron transfer rates, resulting in greater $^{\bullet}OH$ yields compared to unmodified SnO_2 [77]. Collectively, these strategies highlight OVs engineering is an effective approach to tune the electronic structure of (photo)electrocatalysts and the surface absorption/desorption of reactants toward molecular O_2 activation.

Confining metal particles into the support: Advanced strategies, such as embedding or encapsulating metal particles within porous matrices, have emerged to address challenges like structural collapse and metal leaching during catalytic reactions. For example, Guo *et al.* embedded Fe_2O_3 nanoparticles directly into the framework of a carbon nanotube (CNT) filter, termed Fe_2O_3-in-CNT, which reduced iron leaching by a factor of 18.8 compared to a surface-coated counterpart (Fe_2O_3-out-CNT), releasing only 1.6×10^{-2} mg/L of iron *vs.* 0.3 mg/L [78]. Beyond enhancing catalyst durability, spatial confinement within support materials can reshape reaction mechanisms. The embedded configuration improved ROS generation by enabling *in situ* H_2O_2 production and its conversion to $^1O_2$ *via* iron redox cycling. In contrast, the surface-coated filter primarily generated $^{\bullet}OH$, highlighting how nanoparticle stability and spatial arrangement influence ROS pathways (Fig. 4E). Such findings emphasize the critical role of nanostructure engineering in directing molecular O_2 activation.

Collectively, the strategies outlined above target the primary mechanisms of (photo)electrocatalyst deactivation: metal leaching, particle agglomeration/sintering, and structural collapse of the support. By mitigating these failure modes, these approaches significantly enhance operational longevity, which is paramount for the practical implementation of (photo)electrocatalytic processes in environmental remediation.

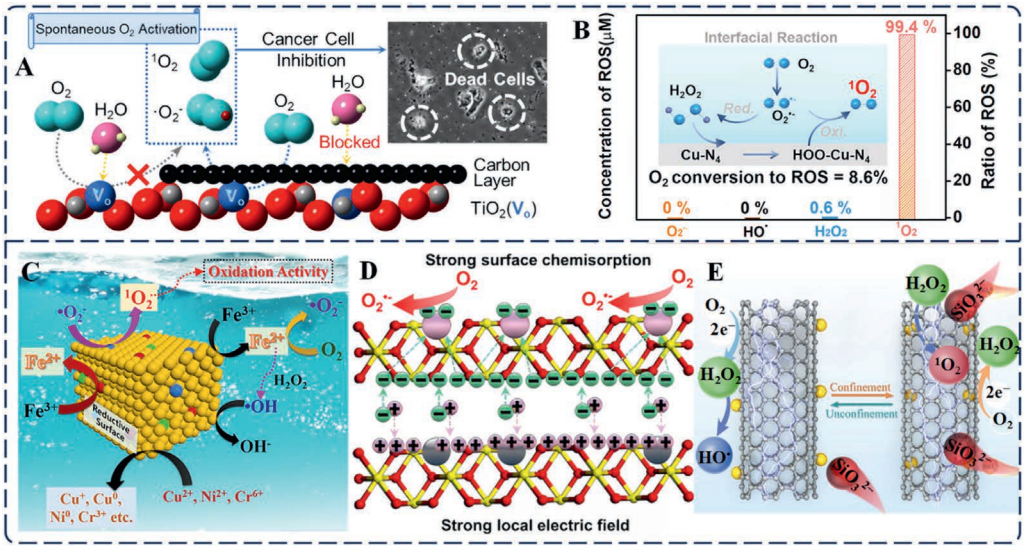


Fig. 4. (A) Self-driven ROS generation from O_2/H_2O molecules *via* interfacial oxygen vacancies on carbon-coated TiO_{2-x}. Copied with permission [71]. Copyright 2020, ACS. (B) The scheme for O_2 to $^1O_2$ and the ratio of O_2 to individual ROS in the SA-$Cu_{1.0}$CA electrocatalytic system. Copied with permission [73]. Copyright 2023, ACS. (C) Illustration of $^1O_2$ triggered by $O_2^{\bullet-}$ in the Mo cocatalytic Fenton reaction with enhanced REDOX activity. Copied with permission [74]. Copyright 2019, ACS. (D) Illustration of O_2 to $O_2^{\bullet-}$ by synergy of dual defects in cubic BiO_{2-x}. Copied with permission [76]. Copyright 2019, Wiley. (E) Possible activation mechanism of molecular O_2 in the Fe_2O_3-in-CNT and Fe_2O_3-out-CNT system. Copied with permission [78]. Copyright 2021, ACS.

5. (Photo)electrocatalytic device for molecular O_2 activation

The development of stable and efficient photo(electro)catalytic system is one of the important components to industrial applications. The ideal device for molecular O_2 activation must balance key factors: sufficient active sites and efficient mass transfer to sustain high reaction rates.

5.1. Flow-by (photo)electrochemical systems

Conventional (photo)electrocatalytic approaches for ROS generation typically rely on stirred reactors with suspended catalyst powders, which require continuous molecular O_2 supply to maintain reaction efficiency. While effective in laboratory settings, these systems face practical limitations, including inefficient mass transfer, catalyst aggregation and recovery during prolonged operation [79,80]. To address these drawbacks, recent advancements have focused on immobilizing catalyst, such as fixed-bed reactors or electrode-integrated platforms. These configurations not only prevent catalyst loss and simplify reuse but also enhance scalability for real-world applications. For example, Fuku *et al.* developed a dual-compartment solar-driven reactor using a $WO_3/BiVO_4$ photoanode and an Au cathode [81]. This solar-driven dual-compartment system enables simultaneous H_2O_2 generation at both electrodes without requiring external voltage, with the photoanode and cathode achieving Faradaic efficiencies of 50 % and 90 % for H_2O_2 production, respectively. In a separate study, Zhou *et al.* demonstrated that immobilized $BiVO_4$-based composites functionalized with silver or copper nanoparticles generated $^{\bullet}OH$ and $O_2^{\bullet-}$ at rates of 371 and 292 $\mu mol\, g^{-1}\, h^{-1}$, respectively in an H-cell reactor separated by a Nafion 115 ion exchange membrane (Fig. 5A) [82]. A critical advantage of immobilized systems lies in their inherent charge-directed pollutant migration. Positively charged contaminants are electrostatically attracted to the negatively charged cathode, while anionic species migrate toward the photoanode. This directional transport ensures continuous adsorption of pollutants onto the electrode surfaces, where they undergo oxidative degradation *via in situ*-generated ROS. Such mechanisms not only enhance degradation efficiency but also minimize energy losses associated with random diffusion in conventional slurry reactors. By replacing suspended catalysts with immobilized architectures, researchers have resolved longstanding challenges in catalyst stability, recyclability, and energy efficiency, paving the way for scalable, energy-efficient ROS generation systems for environmental remediation.

5.2. Flow-through (photo)electrochemical systems

Flow-through (photo)electrochemical systems have emerged as a paradigm shift in molecular O_2 activation for ROS generation, addressing critical limitations of traditional flow-by configurations, including inefficient mass transport, sluggish reaction kinetics, and unstable electrode performance [83,84]. By integrating layered membrane architectures, these systems create confined reaction zones at the nanoscale, where optimized electrical and hydrodynamic interactions minimize diffusion barriers, key features for practical environmental applications (Fig. 5B) [85]. A notable innovation in this field is the Sb-Fe/MXene Janus filter, which features a Ni-foam with spatially separated functional layers: a photocatalytic side (Sb single atoms on MXene) and an electrocatalytic side (Fe nanoclusters on MXene) [86]. The photocatalytic side drives water oxidation *via* a $4e^-$ pathway to generate O_2, while concurrently enabling non-sacrificial H_2O_2 production *via* a $2e^-$ oxygen reduction process. On the opposing side, the electrocatalytic side mediates Fe(III)/Fe(II) cycling, sustaining $^{\bullet}OH$ generation through H_2O_2 dissociation (Fig. 5C). Further progress has been achieved through microporous (photo)electrocatalytic membranes, such as those developed by Kumari *et al.*, where TiO_2 and ZnO coatings are deposited onto porous stainless-steel substrates using atomic layer deposition (Fig. 5D) [87]. These membranes suppress electron-hole recombination during (photo)electrocatalysis, significantly boosting the production of $^{\bullet}OH$ and $O_2^{\bullet-}$. Operation in the flow-through configuration outperformed the conventional batch reactor model ($k = 0.17\ min^{-1}$) due to convection-enhanced mass transport. As compared to a conventional batch reactor, the flow-through (photo)electrochemical system exhibited $>$ 4 times higher oxidation flux due to the convection-enhanced mass transfer and improved catalyst stability [84]. Such engineered decoupling of redox reactions not only enhances molecular O_2 activation efficiency but also ensures long-term stability under

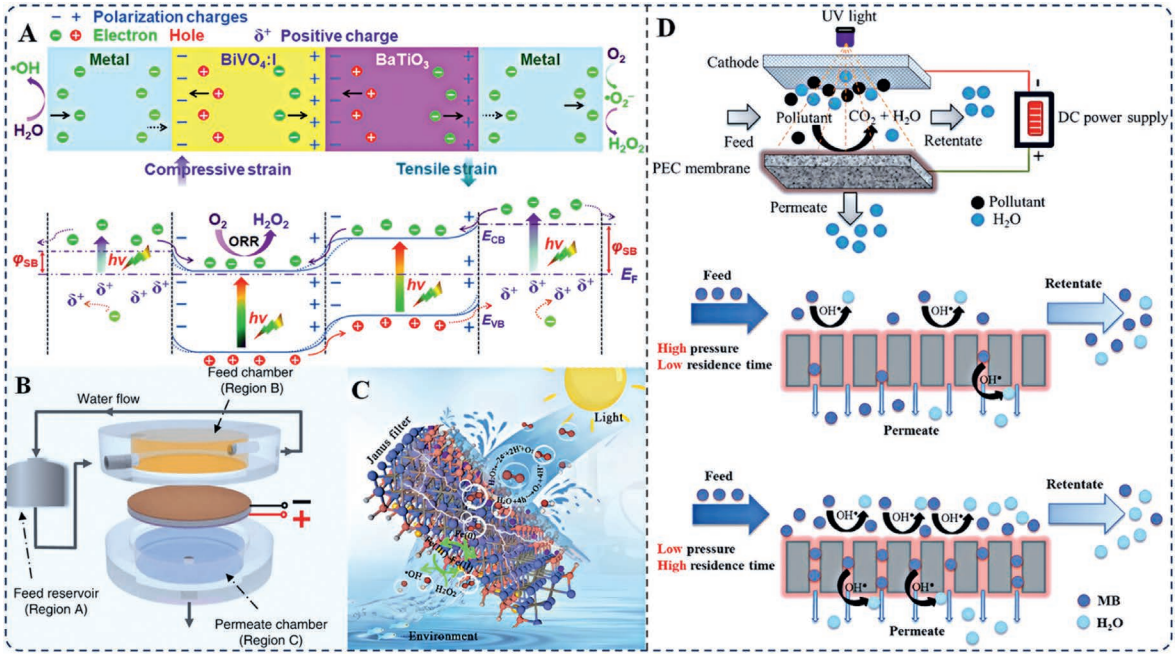


Fig. 5. (A) Illustration of charge transfer processes for ROS generation on a flow-by BiVO4:I/BTO-metal electrode. Copied with permission [82]. Copyright 2021, Wiley. (B) Schematic illustrating the cross-flow filtration system. Copied with permission [85]. Copyright 2020, Springer Nature. (C) Schematic of the Sb-SA/MXene photocatalytic surface with H_2O_2 generation and the Fe-NC/MXene electrocatalytic surface with •OH production concurrently. Copied with permission [86]. Copyright 2023, Elsevier. (D) The (photo)electrocatalysis assisted filtration process occurring in the interaction of pollutant solute and reactive oxygen species generated in cross flow filtration mode. Copied with permission [87]. Copyright 2022, Elsevier.

continuous operation, underscoring their viability for scalable environmental remediation technologies.

6. Application in environmental protection

The activation of molecular O_2 to generate ROS has gained significant attention in environmental remediation due to its cost-effectiveness, eco-friendly nature, and potent oxidative capacity, offering a sustainable alternative to conventional remediation methods.

6.1. Pollutants degradation

Persistent organic pollutants, including antibiotics and pharmaceuticals, threaten ecosystems and human health due to their resistance to natural degradation [88]. Central to this process is the identification of molecular sites to oxidative attack. Computational tools like the Fukui index provide critical insights by quantifying atomic reactivity within a molecule [89]. Three indices are pivotal:

$$\text{Nucleophilic attack index } f^{+} = q(\mathrm{N}+1) - q(\mathrm{N}) \quad (1)$$

$$\text{Electrophilicity attack index } f^{-} = q(\mathrm{N}) - q(\mathrm{N}-1) \quad (2)$$

$$\text{Free radical attack index } f^{0} = 1/2[q(\mathrm{N}+1) - q(\mathrm{N}-1)] \quad (3)$$

where q represents the electron density of the atom, and the electron density values q(N), q(N-1) and $q(N+1)$ are derived from Natural Bond Orbital charge calculations [3]. Regions with higher f^{+} or f^{0} values are prone to nucleophilic radicals like •OH, while sites with elevated f^{-} value are targeted by electrophilic species such as $^1O_2$. For example, computational analyses of the antibiotic tetracycline (TC) reveal that •OH radicals preferentially attack C, O, and N atoms (*e.g.*, C8, O23, N29), forming hydroxylated intermediates. Simultaneously, $O_2^{\bullet-}$ cleave critical bonds at high-f^{0} sites (*e.g.*, C7, O23, N29), initiating ring-opening reactions at positions such as C16 and C18. These fragmented intermediates are further oxidized to harmless end products like CO_2 and H_2O [11]. Recent advances highlight the synergy between experimental systems and computational modeling. For instance, a TiO_2 photoanode with engineered surface facets demonstrated enhanced cleavage of resilient carbon-fluorine bonds in fluorinated pollutants under (photo)electrocatalytic conditions, leveraging •OH radicals for efficient degradation [90]. Demonstrating practical applicability, a modified biochar electrocatalytic system achieved effective degradation of diverse emerging contaminants in real wastewater [91]. Driven primarily by •OH, $O_2^{\bullet-}$, and $^1O_2$ generation from molecular O_2 activation, removal efficiencies reached 59.2 % (antibiotics), 89.2 % (quinoline), 88.3 % (atrazine), and 100 % (bisphenol A) within a 5 h treatment period. Such integrated approaches enable precise targeting of pollutants, underscoring the potential of ROS-mediated pollutants remediation.

6.2. Sterilization and disinfection

Traditional sterilization and disinfection methods, such as chlorine, ozone, or persulfate treatments, often produce harmful chemical byproducts, posing risks to ecosystems and human health [92]. In response, ROS generated through (photo)electrocatalytic activation of molecular O_2 have emerged as a safer, residue-free alternative, aligning with the growing demand for sustainable solutions in environmental remediation [93,94]. Materials such as metals (*e.g.*, Ag, Cu), metal oxides (*e.g.*, TiO_2, CuO, Fe_2O_3, ZnO), and carbon-based structures (*e.g.*, graphene oxide, carbon nanotubes) can efficiently activate molecular O_2 for ROS generation to disrupt microbial cells while reducing ecological risks. For example, Shi *et al.* designed a (photo)electrochemical system that combines light-driven oxidation with on-site H_2O_2 production, powered by renewable energy, to disinfect water contaminated with *Escherichia*

coli [95]. This flow-through method achieved bacterial inactivation rates 2.19 times higher than conventional electrochemical H_2O_2 production and 2.11 times greater than standalone flow-by processes, highlighting the enhanced efficiency of ROS-mediated mechanisms such as h^+, $^{\bullet}OH$, $O_2^{\bullet-}$. Further demonstrating the resilience of ROS-based systems, Valenzuela *et al.* demonstrated the capacity of electrospray TiO_2/Ce-TiO_2/graphene oxide anodes in a (photo)electrocatalytic arrangement to inhibit bacterial growth and boost ROS generation even under the very unfavorable conditions [96]. By leveraging renewable energy to eliminate harmful byproducts and, this approach offers a promising pathway for advancing environmental remediation technologies.

6.3. Volatile organic compounds (VOC) oxidation

Unlike pollutants dissolved in water, the effective elimination of gas-phase VOCs necessitates managing complex multiphase interactions (gas, liquid, solid) [97]. A critical prerequisite for degradation *via* ROS is the efficient transfer of VOCs from exhaust streams to the gas-liquid interface, followed by their dissolution into the aqueous phase. Crucially, because VOC oxidation operate continuously, ROS generation must occur rapidly and with sufficient persistence to sustain the degradation process, a stark contrast to batch-based treatments used for water pollutants. For example, Qiao *et al.* developed a (photo)electrocatalytic system that integrates a gas-permeable electrode with a light-responsive anode, effectively converting toxic H_2S into benign sulfur and H_2O_2 [98]. This design achieved rapid molecular O_2 diffusion and selective $2e^-$ ORR, enabling a high H_2O_2 production rate of $0.8\ mmol\ L^{-1}\ h^{-1}$ at the cathode. Meanwhile, the anode fully oxidized H_2S to sulfur using an iodide-based mediator, recovering sulfur at 0.60 mmol/h. Thus, the gas diffusion electrode was pivotal in this process, establishing optimized gas/water interfaces within its porous structure. This configuration significantly enhances the transport of electrons, ions, and gaseous reactants, thereby accelerating reaction kinetics. Furthermore, the formation of gas cavities adherent to the electrode surface can promote the more effective oxidation of dissolved species. Collectively, such engineered interfaces enable continuous VOC degradation *via* ROS-driven mechanisms, providing a promising foundation for scalable and sustainable strategies to mitigate gas-phase environmental pollutants.

6.4. Soil preservation

Great concern has been paid to polycyclic aromatic hydrocarbons (PAHs) polluted soil because they can enter the food chains and post health risks on ecological receptors [99]. However, conventional methods require substantial exogenous supplies of H_2O_2, incurring high costs and logistical challenges related to its procurement, transport, and storage. To address these limitations, (photo)electrocatalytic *in-situ* H_2O_2 generation has emerged as a critical advancement. Particularly, gas diffusion electrodes consisting of a catalyst layer and a diffusion layer have been just developed in last decade, which can continuously produce H_2O_2 *via* $2e^-$ ORR, offering significant potential for environmental remediation. Chu *et al.* engineered a modified ordered mesoporous carbon-based gas diffusion electrode, which can *in-situ* produce H_2O_2 and further to generate $^{\bullet}OH$ radicals locally [100]. The practicability of the system was further validated using a contaminated soil spiked with anthracene, pyrene, and benzanthracene; remediation efficiency was quantified, and PAH degradation pathways were elucidated. Additionally, ROS exert a dual influence on soil carbon cycling: They enhance organic matter mineralization while simultaneously promoting long-term carbon stabilization through increased recalcitrance of residual organic matter and organo-mineral complex formation [101]. Consequently, understanding ROS generation from molecular O_2 activation and their subsequent effects on organic matter transformation represents an emerging research frontier, providing fundamental chemical insights into oxidative enzymatic processes central to soil biogeochemistry.

7. Conclusions and outlook

This review comprehensively examines the molecular O_2 activation pathways in (photo)electrocatalytic systems and elucidates the mechanisms driving ROS generation. By highlighting efficient ROS-producing catalysts, we clarify correlations between activation routes and dominant ROS species while establishing a framework for optimizing catalyst design and reaction device. To bridge lab-scale innovations and industrial deployment, future work must address four key challenges:

(1) Scalable catalyst synthesis. While oxygen vacancy engineering, heterojunctions, and doping enhance molecular O_2 activation, these strategies face intrinsic constraints: doping may block active sites, and facet engineering often involves complex syntheses. Prioritizing scalable, low-cost production of robust catalysts is imperative. Refining synthesis protocols to balance performance with industrial manufacturability will be essential for overcoming efficiency-stability trade-offs, particularly in large-scale environmental or energy applications.
(2) Enhancing ROS yields. The low solubility of molecular O_2 in electrolytes often limits ROS yields in (photo)electrocatalytic processes. Integrating gas diffusion (photo)electrodes to create a stable gas-electrode-electrolyte interface could enhance molecular O_2 transport. Combining computational modeling with catalyst optimization will improve molecular O_2 delivery to catalytic surfaces and promote intermediates desorption, thereby increasing ROS yields.
(3) Advanced reactor engineering. Flow-through configuration offers distinct advantages, significantly enhancing mass transfer and consequently accelerating reaction kinetics while improving electron utilization efficiency. Strategically embedding nanoconfined catalytic architectures within structured (photo)electrodes presents a synergistic pathway to enhance activity, ROS selectivity, and long-term stability.

CRediT authorship contribution statement

Limin Jin: Data curation, Conceptualization. **Jie Xu:** Conceptualization. **Huayue Zhu:** Supervision, Conceptualization. **Chunjuan Li:** Writing – review & editing, Conceptualization. **Zhengfeng Hu:** Supervision, Conceptualization. **Qi Wang:** Writing – review & editing, Formal analysis.

Declaration of competing interest

The authors declare that they have no known competing financial interest or personal relationships that could have appeared to influence the work reported in this paper.

Acknowledgments

This work was financially supported by the National Natural Science Foundation of China (No. 22276168) and “Pioneer” and “Leading Goose” R&D Program of Zhejiang (No. 2025C02240).

References

[1] X. Zhou, X. Li, Y. Xiang, et al., Chin. Chem. Lett. 36 (2025) 110664.

[2] J. Guo, B. Gao, Q. Li, et al., Adv. Mater. 36 (2024) 2403965.
[3] L.M. Jin, S.J. You, X.G. Duan, et al., J. Hazard. Mater. 423 (2022) 127111.
[4] K. Lu, T. Ren, N. Yan, et al., Environ. Sci. Technol. 57 (2023) 18888–18897.
[5] Z. Wang, N. Hu, L. Wang, et al., Angew. Chem. Int. Ed. 63 (2024) e202407628.
[6] S. Nazia, N. Sahu, V. Jegatheesan, et al., Chem. Eng. J. 412 (2021) 128598.
[7] J.M. Anglada, M.Martins Costa, J.S. Francisco, M.F. Ruiz López, Acc. Chem. Res. 48 (2015) 575–583.
[8] L.L. Zhou, Y.T. Liu, H. Shi, et al., Water Res. 250 (2024) 121075.
[9] S. Yang, S. Sun, Z. Xie, et al., Environ. Sci. Technol. 58 (2024) 19571–19583.
[10] H. Yi, E. Almatrafi, D. Ma, et al., Water Res. 233 (2023) 119719.
[11] Q. Li, F.T. Li, Chem. Eng. J. 421 (2021) 129915.
[12] Q. Li, Q. Zhou, Y. Wu, et al., J. Environ. Chem. Eng. 155 (2025) 111–126.
[13] J. Chang, B. Yu, X. Peng, et al., Water Res. 272 (2025) 122960.
[14] Q. Li, M. Deng, J. Gao, et al., Sep. Purif. Technol. 362 (2025) 131722.
[15] Q. Wang, Y. Hui, X. Ma, et al., Chem. Eng. J. 507 (2025) 160487.
[16] H. Zhang, J. He, C. Zhai, M. Zhu, Chin. Chem. Lett. 30 (2019) 2338–2342.
[17] L. Jin, Y. Wang, Q. Li, et al., Appl. Catal. B: Environ. 373 (2025) 125328.
[18] K. Wang, Y. Li, G. Zhang, et al., Appl. Catal. B: Environ. 240 (2019) 39–49.
[19] H.Y. Gu, X. Liu, X.F. Liu, et al., Nat. Commun. 12 (2021) 5422.
[20] Y. Wang, H. Li, Y. Chen, et al., Appl. Catal. B: Environ. 374 (2025) 125388.
[21] X.Y. Li, H.Y. Chu, P. Wang, et al., Sep. Purif. Technol. 372 (2025) 133525.
[22] Q. Wang, L. Ren, J. Zhang, et al., Adv. Energy Mater. 13 (2023) 2301543.
[23] R. Long, H. Huang, Y. Li, et al., Adv. Mater. 27 (2015) 7025–7042.
[24] R. Long, K. Mao, X. Ye, et al., J. Am. Chem. Soc. 135 (2013) 3200–3207.
[25] X. Lu, X. Zhou, W. Qiu, et al., J. Hazard. Mater. 438 (2022) 129420.
[26] X. Xiao, Z. Ruan, Q. Li, et al., Adv. Mater. 34 (2022) 2200612.
[27] Y. Wang, Y. Lin, S. He, et al., J. Hazard. Mater. 461 (2024) 132538.
[28] M.C. DeRosa, R.J. Crutchley, Coord. Chem. Rev. 233-234 (2002) 351–371.
[29] J. Al-Nu'airat, I. Oluwoye, N. Zeinali, et al., Chem. Rec. 21 (2021) 315–342.
[30] S. Jiang, M. Xie, L. Jin, et al., Chin. Chem. Lett. 36 (2025) 110293.
[31] J. Xie, C. Zhang, T.D. Waite, Water Res. 217 (2022) 118425.
[32] F. Xiao, Z.N. Wang, J.Q. Fan, et al., Angew. Chem. Int. Ed. 60 (2021) 10375–10383.
[33] Y. Kim, H. Lee, H. Oh, et al., Environ. Sci. Technol. 56 (2022) 5763–5774.
[34] C. Chu, Z. Chen, D. Yao, et al., Angew. Chem. Int. Ed. 63 (2024) e202317214.
[35] Q. Wang, A. Liu, B. Shen, et al., Chem. Eng. J. 502 (2024) 157806.
[36] Q. Zhu, Y. Shi, Y. Tao, et al., Chem. Eng. J. 482 (2024) 149066.
[37] J.H. Lee, D.Y. Jo, J.W. Choung, et al., J. Hazard. Mater. 403 (2021) 124085.
[38] Q. Zhang, G. Li, W. Liu, et al., Appl. Catal. B: Environ. 352 (2024) 124051.
[39] X. Quan, F. Guo, R. Li, et al., ACS Appl. Nano Mater. 7 (2024) 23228–23239.
[40] Y. Yang, X. Yang, L. Tang, et al., Adv. Mater. 37 (2025) 2502321.
[41] C.H. Choi, M. Kim, H.C. Kwon, et al., Nat. Commun. 7 (2016) 10922.
[42] G. Zhang, R. Hao, J. Zhang, et al., J. Colloid Interface Sci. 658 (2024) 301–312.
[43] Y. Shang, X. Xu, B. Gao, et al., Chem. Soc. Rev. 50 (2021) 5281–5322.
[44] Y. Yang, Y. Yang, Z. Pei, et al., Matter 3 (2020) 1442–1476.
[45] H. Jeong, S. Shin, H. Lee, ACS Nano 14 (2020) 14355–14374.
[46] H. Li, T. Li, R. Zhao, et al., Small 21 (2025) 2412234.
[47] H. Li, H. Ji, J. Liu, et al., Appl. Catal. B: Environ. 328 (2023) 122481.
[48] J. Zhang, H. Yang, B. Liu, Adv. Energy Mater. 11 (2021) 2002473.
[49] J. Zhang, Z. Zhou, Z. Feng, et al., Environ. Sci. Technol. 56 (2022) 1331–1340.
[50] Y. Qin, R. Tan, J. Wen, et al., Chem. Sci. 14 (2023) 7346–7354.
[51] S. Liu, D. Lu, X. Wang, et al., J. Mater. Chem. B 5 (2017) 4918–4925.
[52] J. Liu, Z. Yao, G. Qiu, et al., Chem. Eng. J. 455 (2023) 140602.
[53] A. Liu, X. Ma, B. Shen, et al., Chem. Eng. J. 504 (2025) 158929.
[54] D. Iglesias, A. Giuliani, M. Melchionna, et al., Chem 4 (2018) 106–123.
[55] C.Y. Chen, C.T. Jafvert, Environ. Sci. Technol. 44 (2010) 6674–6679.
[56] H. Braun, D. Mitoraj, J. Kuncewicz, et al., Appl. Catal. A: Gen. 660 (2023) 119173.
[57] L. Wang, H. Du, X. Wang, et al., Environ. Res. 272 (2025) 121166.
[58] H. Wang, C. Yang, F. Chen, et al., Angew. Chem. Int. Ed. 61 (2022) e202202328.
[59] S. Huang, B. Zhang, D. Wu, et al., Appl. Catal. B: Environ. 340 (2024) 123216.
[60] Z. Feng, Q. Tian, Q. Yang, et al., Appl. Catal. B: Environ. 286 (2021) 119908.
[61] M. Sun, B. Liu, W. Han, et al., Appl. Catal. B: Environ. 304 (2022) 120980.
[62] H. Zhan, Q. Zhou, M. Li, et al., Appl. Catal. B: Environ. 310 (2022) 121329.
[63] Y. Peng, W. Xiao, H. Wang, Z. Bian, Appl. Catal. B: Environ. 363 (2025) 124820.
[64] B. Huo, F. Meng, J. Yang, et al., Chem. Eng. J. 436 (2022) 135173.
[65] J. Zhang, X. Chang, Z. Luo, et al., Chem. Commun. 54 (2018) 7026–7029.
[66] J. Zhang, G. Zhang, H. Lan, et al., Environ. Sci. Technol. 57 (2023) 1134–1143.
[67] Z. Lv, L. Kang, X. Pan, et al., ACS Catal. 14 (2024) 10172–10180.
[68] J.H. Baek, T.M. Gill, H. Abroshan, et al., ACS Energy Lett. 4 (2019) 720–728.
[69] K. Liu, Y. Wang, F. Liu, et al., Chem. Eng. J. 473 (2023) 145292.
[70] A. Li, H. Qiu, Z. Wang, et al., ACS Sustain. Chem. Eng. 12 (2024) 9558–9567.
[71] P. Lyu, J. Zhu, C. Han, et al., ACS Appl. Mater. Interfaces 13 (2021) 2033–2043.
[72] Y. Zhang, J. Zhang, B. Zhang, et al., Nat. Commun. 11 (2020) 558.
[73] Z. Feng, M. Chen, Q. Yang, et al., Environ. Sci. Technol. 57 (2023) 17123–17131.
[74] Q.Y. Yi, J.H. Ji, B. Shen, et al., Environ. Sci. Technol. 53 (2019) 9725–9733.
[75] Y. Rao, Y. Zhang, J. Fan, et al., Chem. Eng. J. 435 (2022) 134882.
[76] Y. Mao, P. Wang, L. Li, et al., Angew. Chem. Int. Ed. 59 (2020) 3685–3690.
[77] C. Yang, S.S. Shang, X.Y. Li, J. Hazard. Mater. 436 (2022) 129212.
[78] D. Guo, Y. Liu, H. Ji, et al., Environ. Sci. Technol. 55 (2021) 4045–4053.
[79] S. Dominguez, P. Ribao, M.J. Rivero, I. Ortiz, Appl. Catal. B: Environ. 178 (2015) 165–169.
[80] S. Qing, X. Lu, Y. Jiang, et al., Chin. Chem. Lett. 37 (2026) 110576.
[81] K. Fuku, Y. Miyase, Y. Miseki, et al., Chem.-Asian J 12 (2017) 1111–1119.
[82] X. Zhou, B. Shen, J. Zhai, N. Hedin, Adv. Funct. Mater. 31 (2021) 2009594.
[83] M. Sun, X. Wang, L.R. Winter, et al., ACS ES&T Eng. 1 (2021) 725–752.
[84] Y.B. Liu, G.D. Gao, C.D. Vecitis, Acc. Chem. Res. 53 (2020) 2892–2902.
[85] Y.M. Zhao, M. Sun, X.X. Wang, et al., Nat. Commun. 11 (2020) 6228.
[86] L. Jin, M. Sun, J. Yang, et al., Appl. Catal. B: Environ. 339 (2023) 123150.
[87] P. Kumari, N. Bahadur, X.A. Conlan, et al., Water Res. 218 (2022) 118519.
[88] S. Naghdi, M.M. Shahrestani, M. Zendehbad, et al., J. Hazard. Mater. 442 (2023) 130127.
[89] J. Guo, H. Sun, X. Yuan, et al., Water Res. 219 (2022) 118558.
[90] H. Chi, J. Ma, R. Duan, et al., Water Res. 262 (2024) 122101.
[91] S. Qu, H. Yang, R. Wang, et al., Sep. Purif. Technol. 371 (2025) 133288.
[92] Z. Tang, R. Yin, W. Qu, et al., ACS ES&T Eng. 2 (2022) 629–641.
[93] N. Kaushik, S. Mitra, E.J. Baek, et al., J. Adv. Res. 43 (2023) 59–71.
[94] Y. Fu, J. Chi, Y. Wu, et al., Appl. Surf. Sci. 692 (2025) 162711.
[95] Y. Shi, Y. Qian, J. Guo, et al., J. Clean Prod. 416 (2023) 138001.
[96] L. Valenzuela, M. Faraldos, A. Bahamonde, R. Rosal, Electrochim. Acta 395 (2021) 139203.
[97] Z. Jiang, Y. Wang, C. Chen, et al., Chin. Chem. Lett. 35 (2024) 109400.
[98] L. Qiao, J. Bai, T. Luo, et al., Appl. Catal. B: Environ. 238 (2018) 491–497.
[99] S.P. Maletić, J.M. Beljin, S.D. Rončević, et al., J. Hazard. Mater. 365 (2019) 467–482.
[100] L. Chu, L. Cang, G. Fang, et al., J. Hazard. Mater. 428 (2022) 128273.
[101] G.H. Yu, Y. Kuzyakov, Earth Sci. Rev. 214 (2021) 103525.